NJC

ROYAL SOCIETY OF CHEMISTRY

PAPER

Cite this: *New J. Chem.*, 2021, **45**, 18459

Synthesis of an unprecedented H-stitched binuclear crystal structure based on selective fluorescence recognition of Zn^{2+} in newly synthesized Schiff base ligand with DFT and imaging application in living cells†

Soumya Sundar Mati, *[a] Saugata Konar [b] and Boby Samai [c]

A zinc coordinated rare binuclear complex was synthesised and characterized by elemental analysis and single-crystal X-ray diffraction. Two mononuclear units formed by two Schiff base ligands 2-((2-(pyrimidin-2-yl)hydrazono)methyl)phenol (PHP) coordinated with zinc ion are bonded together through a hydrogen atom to form the binuclear complex. Only a single H atom significantly linked the two giant mononuclear units to form this rare complex structure. Hydrogen bonding interactions and C–H···π interactions in the crystallographic binuclear complex result in a giant supramolecular assembly. In the solution, the PHP bound Zn^{2+} complex was investigated by several experimental procedures including UV-Vis absorption, steady state as well as time resolved fluorescence, proton NMR spectra and theoretical calculations to explain the response. NMR spectra clearly clarified the binding location and role of functional groups using the direct and neighbouring protons. Density functional theory explained the step by step formation of the H stitched binuclear complex from ligand PHP to validate the experimental outcomes. PHP selectively recognises Zn^{2+} by fluorescence "turn-on" owing to the formation of the complex in the solution. During the fluorescence study, the sensitivity was estimated from the slope of the calibration curve, and the detection limit was calculated (0.49 μM) using the 3Sigma method. The ligand is also active to detect *in vitro* Zn^{2+} ion in PC-3 *i.e.*, human prostate carcinoma cells, by Confocal microscope. Therefore, the proposed PHP sensor offers a cost effective compound that can be considered as a viable alternative for Zn^{2+} ion detection and future trials for biophysical applications.

Received 19th July 2021,
Accepted 6th September 2021

DOI: 10.1039/d1nj03471e

rsc.li/njc

Introduction

Among the many significant trace elements in our body, zinc probably draws its maximum attention as the second most important nutrient after Vitamin D, and it appears in the enzymes dispersed all over the human body.[1–3] Zinc derived compounds are extensively used in medical fields as anticancer agents, tumor photosensitizers, radio-protective agents, and antidiabetic insulin mimetic.[1] Apart from this, zinc, the second abundant transition metal ion (2–3 g total in human body) among the physiologically important trace elements performs several roles in human physiopathology.[4–7] Irrespective of such essential usefulness, failure of free zinc ion metabolism can cause harmful neurological diseases, such as Parkinson's disease, amyotrophic lateral sclerosis (ALS), Alzheimer's disease, epilepsy, and ischemia.[8,9] In addition, the excess Zn^{2+} ions present in water and soil may reduce the microbial activity of soil, causing phytotoxic effect and making water muddy and smelly.[5,9] For that reason, the design and development of a selective and noninvasive procedure to detect free zinc ions is still extremely appreciable.

In search of this, a useful complexing agent having the capability of Zn^{2+} ion detection in solution is needed. The main challenges in the design and development of complexing

[a] *Department of Chemistry, Government General Degree College, Keshiary, Paschim Medinipur 721135, India. E-mail: soumyamati@gmail.com*
[b] *Department of Chemistry, The Bhawanipur Education Society College, Kolkata 700020, India*
[c] *Department of Science and Humanities, Hooghly Institute of Technology, Hooghly 712103, India*

† Electronic supplementary information (ESI) available: Fig. S1: ^{1}H NMR of ligand PHP, Fig. S2: HRMS of ligand PHP, Fig. S3: LOD Plot, Table S1: selected bond distances from crystal structure. Scheme S1: mechanism of complex formation. CCDC 1402190 contains the supplementary crystallographic data for complex **1**. For ESI and crystallographic data in CIF or other electronic format see DOI: 10.1039/d1nj03471e

agents to detect Zn^{2+} ions are[10–12] (i) selectivity to zinc ions with respect to other metal ions in such a way that other metal ions may compete for ligand binding sites with zinc ions in solution. (ii) the selectivity of such probes in neutral water based solution. In spite of several zinc sensors,[13,14] Schiff base fluorescent sensors have drawn much attention due to easy synthesis with different sole structures and being very cheap *i.e.* cost effective precursor materials.[12,15–19] Moreover, the nitrogen atom in Schiff base –CH═N moiety has a unique strong attraction to metal ions. Although Schiff bases have some disadvantages such as the hydrolysis of –CH═N bond, less solubility in aqueous solutions, and decomposition tendency in acidic medium causes these bases to be less interesting to some extent in analytical purpose.[20] Moreover, in spite of low yields in many cases and tedious workup,[21] Schiff bases have more and more advantages, including high sensitivity, low cost, easy detection, flexible coordination sites, and easy synthesis protocol.[22,23] The high affinity for the chelation of Schiff bases towards the transition metal ions is utilized in preparing their solid complexes. Schiff base derivatives have played an important role as a chemosensor due to their chromogenic and azomethine groups.[24,25] Therefore, Schiff bases can be applied as a chelating agent for the detection of many metal ions. In addition to sensing, Schiff bases have various other applications in different fields like anti-oxidant, anti-inflammatory, anti-fungal, and anti-cancer agents due to their strong chelating nature.[26] Schiff base-transition metal complexes have also been used as excellent catalysts, antibacterial agents, and effective drugs in the field of pharmacology.[26,27] ICP-MS and ICP-AES (Inductively coupled plasma mass spectroscopy and atomic emission spectroscopy) are well known sensitive detection procedures for several metal ions.[28] The main drawback of these procedures is they detect total metal ions without oxidation state and proper environment of coordination state. Irrespective of that complicated pretreatment, expenses, time consuming, infrastructural backup, and high skill requirements for operation greatly limited their application for routine analysis of myriad samples.[29–31] So, in this scenario, in search of methodical sensitivity, easy-to-use, flexible design, low cost, and experimental simplicity, we are highlighting a simple fluorescence spectroscopic technique for detailed investigation of metal ligand interaction.

Keeping in mind these points, herein, we have introduced a designed Schiff base derivative, 2-((2-(pyrimidin-2-yl)hydrazono) methyl)phenol (PHP), which selectively binds with Zn^{2+} to form a rare fluorescent binuclear complex through a hydrogen atom. According to Pauling, this type of bonds are formed under certain conditions if hydrogen is attracted by rather strong forces to two atoms, instead of one, in order that it may be considered to be acting as a bond between them.[32] In co-ordination chemistry, there are many examples of hydrogen bridge bonds between two metals to form the respective metal complexes,[33–37] but in our case, a hydrogen atom bonded two PHP ligands connects two separate Zn coordinated mononuclear units to form a rare binuclear complex without any metal–metal linkage. Crystallographic structure gives direct evidence in favor of this hydrogen bonded structure. Not only the crystallographic structure but also the overall hydrogen bonding interactions and C–H$\cdots\pi$ interactions are also embodied herein. Moreover, during the complexation, there occurs LMCT, *i.e.*, the ligand to metal charge transfer, and the ligand shows its fluorescence selectivity with Zn^{2+} in the presence of other metal ions. Hence this work consists of detailed spectroscopic observations, including time resolved fluorescence decay and quantum chemical calculations using DFT and TD-DFT (time dependent density functional theory) calculations with the *in vitro* analysis of the ligand and its corresponding complex by human prostate carcinoma (PC-3) cells where most of the earlier reports mentioned either of the above. Therefore, this study demands its complete uniqueness and originality for the synthesis of a new easy to handle, cost effective, and high yield Schiff base compound 2-((2-(pyrimidin-2-yl)hydrazono)methyl)phenol, PHP for Zn^{2+} sensor and separate this metal ion from other liquid metal ion mixture in terms of a new rare crystal structure. The crystal structure is rare as a single H-atom stitched two separate mononuclear units only through the PHP ligands without any metal–metal linkage to form a giant binuclear structure. Therefore, the proposed PHP Schiff base was found to be sensitive, efficient in response spectroscopically as well as biologically, with highly selective sensing performance towards zinc ions at ambient conditions and aqueous pH 7 medium. As per the author's knowledge, this Schiff base PHP sensor is completely new to be applied as a chemical sensor material to form the unique rare binuclear zinc crystal. This approach can be used in the future as a novel way to develop chemo-sensors for application in real environmental and biological samples on a broad scale.

Experimental section

Materials

All the reagents were procured from diverse commercial sources and used without further purification. 2-Chlorolpyrimidine (95%), hydrazine hydrate (50–60%), and salicylaldehyde were purchased from Aldrich, USA and were utilized devoid of any purification. Metal salts such as perchlorate of Na^{+}, K^{+}, Fe^{2+}, Fe^{3+}, Co^{2+}, Cd^{2+}, Hg^{2+}, Pb^{2+}, Ni^{2+}, and Zn^{2+} were purchased from Sigma-Aldrich and used as received. Other metal salts like $LiNO_3$, $Al(NO_3)_3$, $CrCl_3$, $MnCl_2$, and $Cu(ClO_4)_2$ were obtained from Indian based commercial companies. Mili-Q water was used throughout the experiments. For NMR experiments, DMSO-d6 was procured from Sigma-Aldrich, USA.

Synthesis of the ligand (PHP)

Ligand 2-hydrazino pyrimidine, HPym was prepared using the method described in the literature.[38] This ligand PHP was synthesized (Scheme 1) through proper refluxing in ethanolic solution

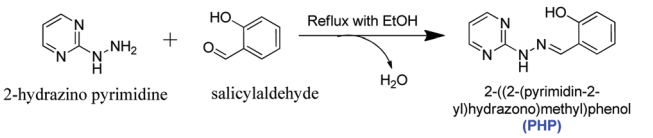

Scheme 1 Synthesis protocol of ligand PHP.

Table 1 Experimental crystallographic data for complex 1

Compound	**1**
Empirical formula	$C_{44}H_{38}Cl_2N_{16}O_{12}Zn_2$
Formula weight	1184.58
Temperature (K)	293(2)
Wavelength (Å)	0.71073
Crystal system	Triclinic
Space group	$P\bar{1}$
Unit cell dimensions	a =13.2000(4)Å b =13.6170(4)Å c = 17.2854(6)Å α = 94.404(2)°, β = 109.640(2)°, γ = 101.574(2)°
Volume (Å^3)	2831.46(15)
Z	2
Density (calc)(Mg m$^{-3)}$	1.389
Absorption coefficient (mm^{-1})	1.011
F(000)	1208
θ range (°) for data collection	1.3, 24.8
Index ranges	$-15 \leq h \leq 15$ $-16 \leq k \leq 16$ $-20 \leq k \leq 20$
Goodness-of-fit on F^2	1.050
Completeness to theta = 25.00°	98.8%
Independent reflections [R_{int}]	9622[0.029]
Refinement method	Full-matrix least squares on F^2
Data/restraints/parameters	9622/0/709
Reflections collected	31720
Final R indices [$I > 2\sigma(I)$]	R_1 = 0.0442, wR_2 = 0.1345
Largest difference peak and hole (e Å^{-3})	−0.35, 0.69

(20 mL) of 2-hydrazino pyrimidine (1.10 g, 10 mmol) with salicylaldehyde (1.22 g, 10 mmol) in EtOH solution (20 mL). After continuous refluxing for 2 h in a water bath, the liquid solution was cooled and left at room temperature for slow evaporation. Finally, the solid compound was separated through a filter, and it was washed repeatedly with ethanol. The desired ligand was then dried over fused $CaCl_2$ (yield: 68%). Furthermore, the ligand PHP has also been synthesized from very cheap precursors under environment friendly experimental conditions and reagents, as mentioned in Scheme 1. Anal. cal. C: 61.67, H: 4.71, N: 26.15, for $C_{11}H_{10}N_4O$: Found: C, 60.64; H, 4.68; N, 26.17. ^{1}H NMR (300 MHz, DMSO-d6): δ 6.75–6.90 (m, aroH), 7.04 (d, J = 8.4 Hz, 1H), 7.19 (t, J = 6.9, 8.4 Hz, 1H), 7.57–7.68 (m, 2H), 8.13 (d, J = 4.8 Hz, 1H), 8.29 (s, 1H), 10.51 (s, 1H), 10.90 (s, 1H) ppm (Fig. S1, ESI†). HRMS: MS-ES$^+$ (m/z): 214.11 (Fig. S2, ESI†).

Preparation of complex 1

At first, 10 mL $Zn(ClO_4)_2{\cdot}6H_2O$ (1 mM, 0.372 g) methanolic solution was dropwise added into a 15 mL solution of PHP (1 mM, 0.214 g) in the same solvent with a 1:1 mole ratio. After continuous stirring for 2 h, the whole solution became yellow. Then, it was kept at room temperature for slow evaporation. Two weeks later, X-ray quality crystals of Complex **1** were separated gently and collected with usual techniques (55.5% yield). Complex **1** is synthesized at room temperature and pressure, and no vigorous condition is needed. Elemental analysis (%) calculated for $C_{44}H_{38}Cl_2N_{16}O_{12}Zn_2$: C, 44.57; H, 3.20; N, 18.91; found: C, 44.54; H, 3.16; N, 18.93.

Crystallographic data collection and refinement

After complete crystallographic study of complex **1**, crystal data has been tabulated in Table 1, and metrical parameters are also inserted in Table S1 (ESI†). Bruker APEX II diffractometer equipped with a normal focus in sealed tube X-ray source with graphite monochromated Mo-Kα radiation (λ = 0.71073 Å) source at 293(2) K in φ and ω scan mode was used for data collection of complex **1**. Also, cell parameter refinement and data decline were performed using Bruker APEX II. Absorption corrections were executed with SADABS. The structure of complex **1** was solved with conventional methods and refined by the full-matrix least square method using F^2 data. For this purpose, SHELXS-97 and SHELXL-97 programmes[39] were used, and anisotropically hydrogen atoms were refined till the complex **1** structure achieved its convergence. Subsequently, methanol as solvent molecules were disordered and removed using SQUEEZE.

Methods

Absorption and emission spectra were recorded using Shimadzu spectrophotometer (UV 1700 model) and spectrofluorimeter (RF 5301 model), respectively, with 1 cm quartz cell. TCSPC (time correlated single photon counting) method was used for fluorescence lifetime measurements through a nanosecond LED at 403 nm as a light source (IBH, LED 07). Data analysis was performed with IBH DAS-6 decay analysis software as conventional methods. Bi-exponential fitting program was used for all fluorescence decay in lifetime measurements as provided by IBH. Elemental analysis results of ligand and metal complex were obtained from PerkinElmer CHN analyzer 2400. Bruker Avance 300 spectrometer was used to obtain proton NMR spectra in DMSO-d6 solvent. The HRMS model XEVO-G2 QTOF YCA 351 mass spectrometer was used to record MS-ESI$^+$ spectra.

Computational

Geometry optimization of ligand PHP and complex **1** was performed using density functional theory, DFT[40] with B3LYP correlation function[41] and 6-31G(d,p) basis set for all atoms. All the structures corresponding to the true minima of the potential energy surface were confirmed by the vibrational frequency calculations. After that TD-DFT *i.e.* time dependent density functional[42,43] theory was applied to calculate electronic transition wavelengths using the same functional and 3-21G basis set. Gaussian 09[44] program package has been used to carry out the calculations.

Cell culture and Fluorescence Imaging

Human prostate carcinoma (PC-3) cell line was obtained from National Centre for Cell Science, Pune, India. After this, it was cultured in RPMI supplemented with 1% PSN antibiotic and 10% FBS (fetal bovine serum) and incubated with 5% CO_2 at 37 °C in a humidified atmosphere. After 75–80% confluence, cells were harvested in the presence of 0.52 mM EDTA and 0.025% trypsin in PBS (phosphate buffered saline) and were seeded at the desired density a day before the experiment to allow them re-equilibrate. The cells were seeded on a 22 mm

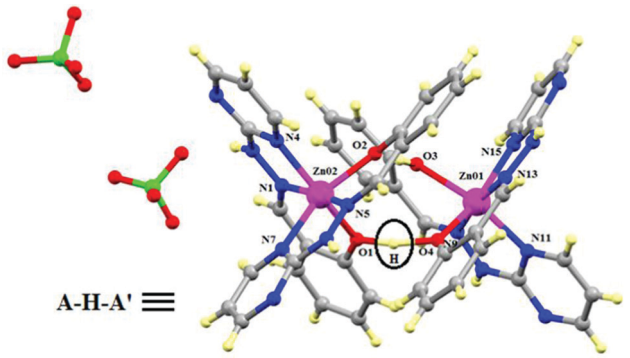

Fig. 1 Perspective view of Complex **1**. The related atoms are only labeled.

cover slip in 6 well plates. Confocal microscope (Olympus) with Andor iXon3 897 EMCCD camera was used for cell imaging at the corresponding excitation of complex **1** and emission under a blue filter.

Result and discussion

Structural description of complex 1

Perspective views with the atom numbering schemes of complex **1** are shown in Fig. 1. Space group $P\bar{1}$ is the crystallization pattern of Complex **1**. Each zinc(II) atom attains a hexa-coordinated distorted octahedral geometry with an N_4O_2 chromophore moiety. For Zn01, the equatorial plane is formed by N9 and N11 from azomethine and pyrimidine nitrogen (N) atoms, respectively, N13 from azomethine N atom of another ligand, O3 from salicyl O atom, and corresponding axial positions are fulfilled by N15 from pyrimidine N atom, O4 from the salicyl O atom. For Zn02, the equatorial plane is formed by N1 and N4 from azomethine N atom and pyrimidine N atom, respectively, N5 from azomethine N atom of another ligand, O1 from salicyl O atom, and rest of the axial positions are fulfilled by N7 from pyrimidine N atom and O2 from the salicyl O atom. Both Zn01 and Zn02 atoms are moved downward 0.007 and 0.018 Å from their respective equatorial planes, *i.e.*, almost lie in that plane. In this binuclear structure, the Zn···Zn separation distance is 5.092 Å. The closest similar conformation of the as-formed chelate (six-member) ring, R1{R1 = Zn02–O2–C16–C17–C18–N5} is the H-form with puckering parameters[45] $q = 0.254(2)$ Å, $\theta = 61.6(7)^\circ$ and $\varphi = 16.3(9)^\circ$. Here, the hydrogen atom stitches the two units (say A and A') to generate a binuclear structure. Generally, O–H bond length is ~ 0.97 Å (from literature survey), but in our complex, the O1–H and O4–H bond lengths are 1.16 Å and 1.34 Å respectively, the O1–H–O4 bond angle is 166.96° likely to be linear. So, both the O1–H and O4–H bond distances are higher than the conventional O–H bond length. It also proves that this H atom binds two mononuclear units A and A′, not solely bound to either of the units. On contrary, H atom connected with O3 is solely bonded with O3 having O3–H bond distance of 0.97 Å, and consequently no covalent bond is observed between O2 and H. Only O2···H hydrogen bond having a distance of 1.49 Å is observed. Hence, the marked H atom (Fig. 1) exclusively ties the knot between two giant mononuclear units A and A′ to form complex **1**. Complex **1** represents different kinds of C–H···π interactions (Fig. 2) (Table 2) in the crystal structure that contribute to the self assembly process. Cg(11), *i.e.*, the pyrimidine ring in the molecule [where Cg(11) is the centre of gravity of the ring (N11–C30–N12–C31–C32–C33)] involved in a C–H···π interaction with symmetry linked aromatic C–H group of C(22) where the distance between Cg(11)···H(22A) is 2.83Å. The chelate ring, Cg(5) [where Cg(5) is the centre of gravity of the ring (Zn01–O3–C23–C28–C29–N9)], again creates C–H···π interaction with symmetry linked aromatic C–H group of C(44) where the distance between Cg(5)···H(44) is 2.89 Å. Lastly, the aromatic C–H group of C(9) where the H(9)···Cg(12) forms C–H···π interaction with symmetry linked aromatic pyrimidine ring Cg(12) [where Cg(12) is centre of gravity of the ring (N15–C41–N16–C42–C43–C44)] of distance 3.49 Å. In general, C–H···π interactions form a 2-D sheet of crystal packing in **1**. Thus in complex **1**, two large Zn coordinated complex structures are joined together only through a H atom to form a rarely observed complex **1**, as seen in the crystallographic study (Fig. 1). In **1**, the perchlorate ions are solely engaged in H-bonding interactions. In the outer coordination sphere, perchlorate ions are involved in intermolecular H-bonding to connect the two units (Fig. 3). Thus a hydrogen

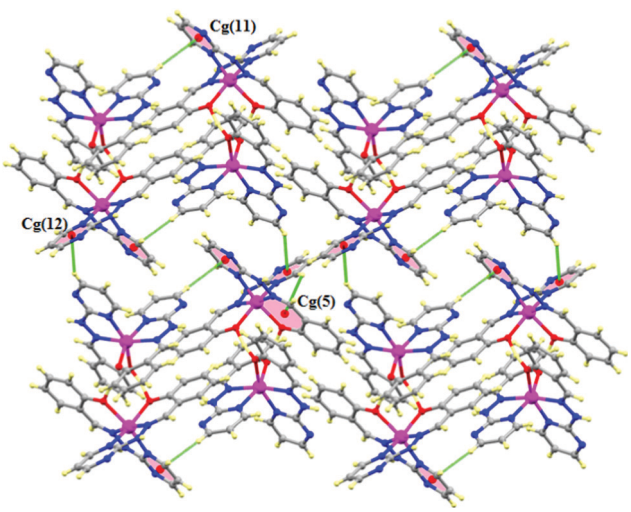

Fig. 2 C–H/π interactions along *a* axis to form 2D sheet.

Table 2 Distances (Å) and Angles (degree) of C–H···π interactions obtained for **1**

Complex	C–H···Cg(Ring)	H···Cg (Å)	C–H···Cg (°)	C···Cg (Å)	Symmetry
Complex **1**	C22–H22···Cg(11)	2.83	148	3.653(7)	$1-X, 1-Y, -Z$
	C44–H44···Cg(5)	2.89	111	3.347(4)	X, Y, Z

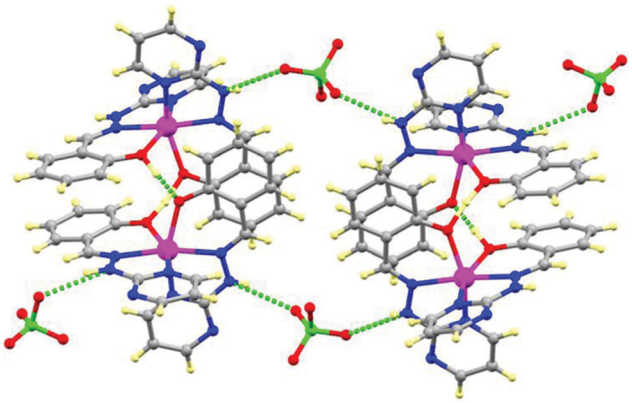

Fig. 3 Dimer formation *via* H-bonding interaction in Complex 1.

Table 3 Hydrogen (H-bond) bond distances (Å) and angles (degree) of Complex **1**

D–H···A	D–H	H···A	D···A	∠D–H···A
N2–H102···O9	0.92(7)	2.11(7)	2.989(7)	160(6)
N6–H106···O6	0.69(3)	2.30(3)	2.960(5)	161(4)
N14–H114···O8	0.58(4)	2.47(4)	3.032(6)	164(4)
O3–H201···O2	0.97(5)	1.49(5)	2.463(3)	179(8)

bonded dimer of complex **1** is formed in which perchlorate ions act as a bridge. The details of H-bonding are given in Table 3.

Absorption

The absorption spectra of the ligand (PHP) and also in the presence of a number of metal cations (*e.g.*, Li^{+}, Na^{+}, Al^{3+}, K^{+}, Cr^{3+}, Mn^{2+}, Fe^{2+}, Fe^{3+}, Co^{2+}, Ni^{2+}, Cu^{2+}, Zn^{2+}, Cd^{2+}, Hg^{2+}, and Pb^{2+}), were taken in a 4 : 1 ACN–buffer solvent mixture (10 mM HEPES buffer, pH = 7) (Fig. 4(a)). The absorption spectrum of the ligand PHP only contains a strong single band at 323 nm, which can be designated to n–π* electronic transition due to the Schiff base moiety.[46] By the addition of various concentrations of zinc metal ion (0–18 μM), the absorption maxima at 335 nm of ligand (PHP) was simultaneously decreased, and a blue shifted new peak at 383 nm was increased through isosbestic points at 356 nm and 292 nm (Fig. 4(b)). Clear isosbestic points specify the existence of only one type of PHP–Zn^{2+} complex. Now, the absorbance at 383 nm of Zn^{2+}–coordinated complex *versus* the equivalent amount of added Zn^{2+} gives a semi-curvature plot (Fig. 4b inset), which shows that 0.5 equivalent of Zn^{2+} is enough to complete the binding with ligand PHP. So this spectral information also coincides with the 1 : 2 metal–ligand crystal structure of complex **1** between Zn^{2+} and PHP.

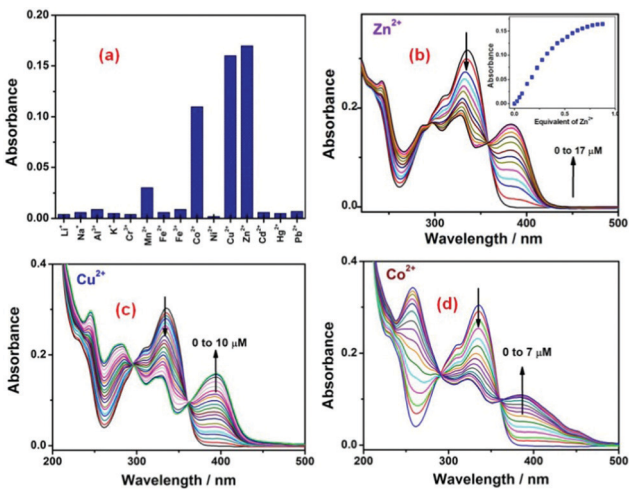

Fig. 4 (a) Absorption bar diagram of different metal ions; absorption titration of PHP with (b) Zn^{2+}(0–17 μM), (c) Cu^{2+} (0–10 μM) and (d) Co^{2+} (0–7 μM) metal ions in 4 : 1 ACN–aqueous buffer medium, inset of (b) absorbance vs equivalence concentration of Zn^{2+}.

Under the same experimental conditions, addition of copper (Cu^{2+}) ion (0–10 μM) to the 4 : 1 ACN–buffer solution of PHP (Fig. 4(c)), a new peak at 393 nm in the absorption spectra appeared progressively with a steady decrease of the initial 335 nm band. Two isosbestic points were noticed during the titrations at 297 nm and 361 nm, which signifies an equilibrium between PHP and Cu^{2+} complex.

Similarly, for Co^{2+} addition (0–7 μM), the absorption band at 335 nm gradually decreased, and simultaneously a new band at 387 nm was raised. With a gradual increase in Co^{2+} concentration, two isosbestic points develop at 360 nm and 291 nm, which is quite clear from Fig. 4(d). The blue shifted absorption spectra of the ligand PHP after the addition of metal ions can be attributed as LMCT (ligand to metal charge transfer). The coordination nature of the metal ion with the ligand through phenolic oxygen atom and the nitrogen atom of Schiff moiety enhances its electron withdrawing capability to show a strong ICT from ligand to metal ion, and consequently, chelate rings are formed.[47,48]

Emission

Fluorescence behaviour of the ligand, *i.e.*, PHP, was monitored upon treatment with different metal ions in 1 : 4 (v/v) aqueous buffer–ACN solvent mixture to verify the suitability of PHP as a selective zinc sensor. Although besides Zn^{2+}, the complex formation also takes place with Cu^{2+} and Co^{2+} individually (as indicated from the absorption study), only the PHP–Zn^{2+} complex is fluorescence active. The fluorescence intensity of PHP was enhanced dramatically upon titration of 0 to 45 μM of Zn^{2+} accompanied by a red-shifted maximal emission peak appearing at 470 nm (Fig. 5a). A very weak emission of the ligand is observed when excited at 383 nm, however fluorescence intensity of PHP at 470 nm is enhanced about 40 fold upon gradual addition of Zn^{2+} whereas the fluorescence intensity change is insignificant in the presence of other metal ions such as Li^{+}, Al^{3+}, Cr^{3+}, Mn^{2+}, Fe^{2+}, Fe^{3+}, Co^{2+}, Ni^{2+}, Cu^{2+}, Mg^{2+}, Cd^{2+}, Hg^{2+}, Pb^{2+} (inset Fig. 5a). This Zn^{2+} bound PHP has also shown high fluorescence even in the presence of all other inspected metal ions (Fig. 5b) to confirm its applicability in any real sample analysis. This remarkable fluorescence enhancement can be explained on the basis of the combined effect of ligand to metal charge transfer (LMCT) and chelation-enhanced fluorescence (CHEF).[49,50] In solution, ligand PHP shows very weak fluorescence due to excited state

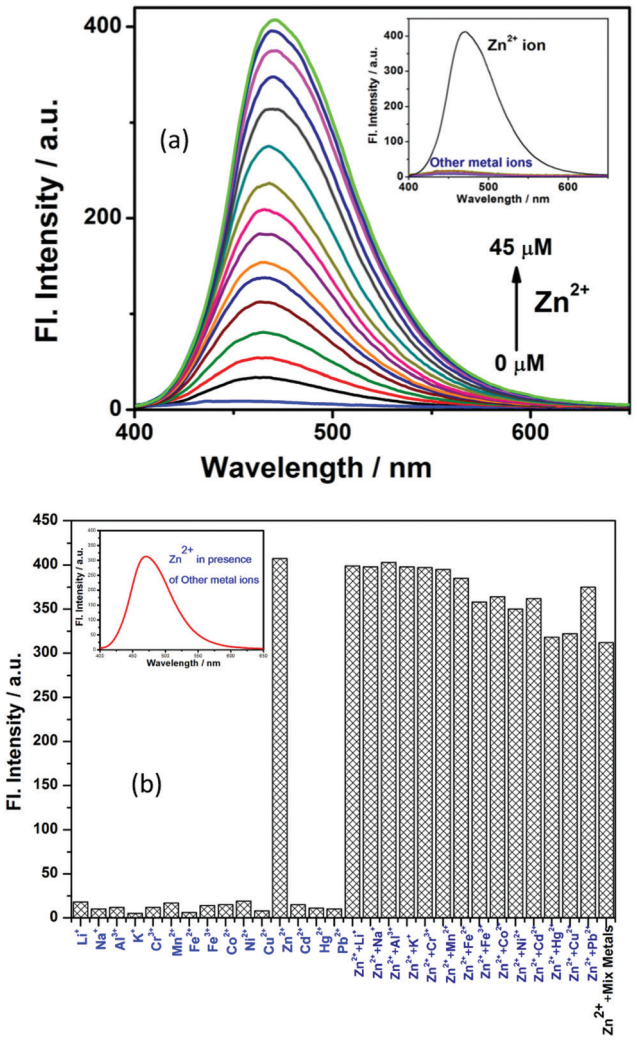

Fig. 5 (a) Fluorescence change of PHP (20 μM) upon addition of zinc ions (0–45 μM) in 4 : 1 ACN–aqueous buffer medium; inset: shows the relative emission of Zn^{2+} over other metals ions, (b) bar diagram indicates the selective binding of Zn^{2+} over other metals ions and PHP–Zn^{2+} emission intensity is not affected in the presence of other individual metal ions and mixed metal ions. Inset: Emission in the presence of all other metal ions.

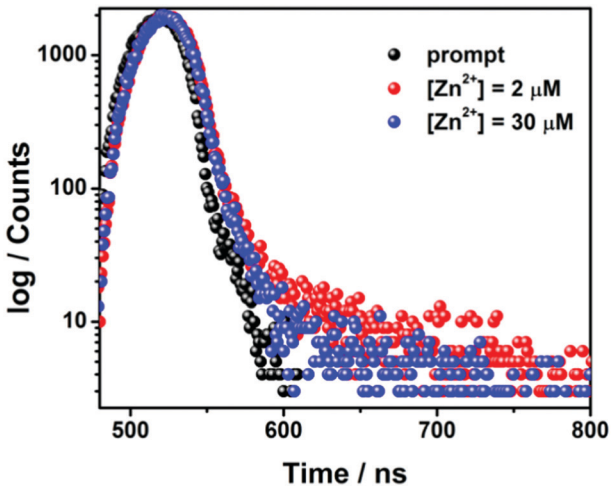

Fig. 6 Lifetime spectra of PHP in the presence of Zn^{2+}.

intramolecular proton transfer (ESIPT) and C=N isomerization. Isomerisation of the C=N bond is the predominant factor in the excited state decay process for the compound.[51] After the addition of Zn^{2+}, the CHEF effect arises when the lone pair on the N coordinates with metal ions such as Zn^{2+}, for which the lone pair is stabilized and consequently inhibits C=N isomerization and ESIPT restoring red shifted fluorescence (Scheme S1, ESI†).[52] The limit of detection (LOD) of Zn^{2+} was calculated as 4.97×10^{-7} M from the 3σ method (Fig. S3, ESI†)[47,53] and quantum yield (ϕ) of the PHP–Zn^{2+} complex is 0.19. The fluorescence intensity of the PHP–Zn^{2+} complex is quenched immediately in the presence of EDTA (ethylenediamine tetra acetic acid), a heavy metal ion chelator. This reveals that PHP coordinates with Zn^{2+} reversibly.

The binding constant K was obtained from the plot of $\log[(F - F_{min})/(F_{max} - F)]$ *vs.* $\log[M]$ in the regression equation[54]

$$\log[(F - F_{min})/(F_{max} - F)] = \log K + n \log[M]$$

where F_{min}, F and F_{max} are the absorption or emission intensities (whichever is applicable) in the absence, presence, and at saturated condition of Zn^{2+}. [M] is the Zn^{2+} ion concentration. The calculated binding constant values for Zn^{2+} bound PHP are 7.58×10^6 and 6.76×10^6 M^{-1} in the ground and excited states, respectively.

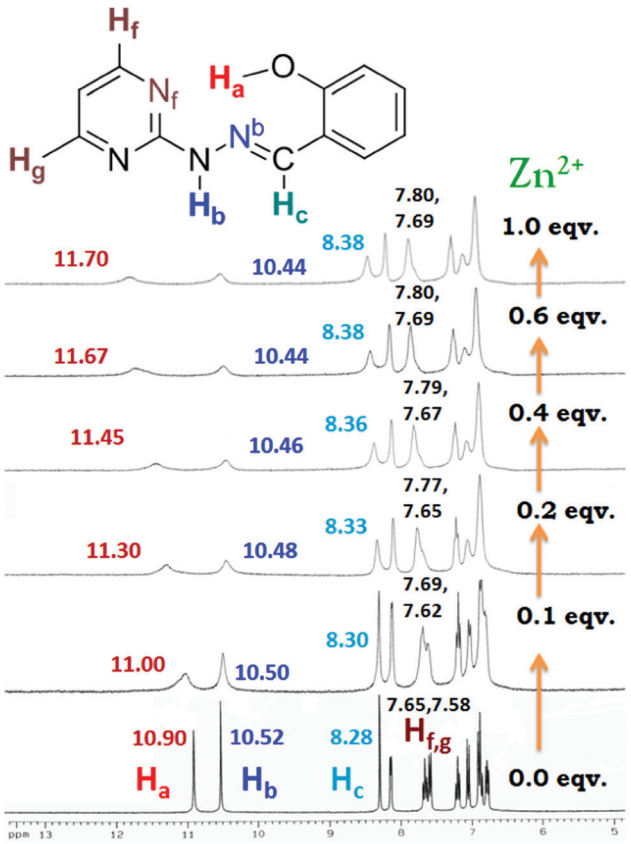

Fig. 7 ^{1}H NMR spectra of PHP upon addition with different equivalents of Zn^{2+} in DMSO-d6. Inset shows the structure of the PHP ligand with specific marking of atoms.

Table 4 Comparison of different properties of PHP with recently reported (a) fluorescent probes (b) nanocomposite and nanoparticle systems

(a)

Schiff base	Sensor type	M : L ratio	pH	Emission wavelength (nm)	Binding constant (M^{-1})	LOD	Application	Ref.
3-Hydroxy-*N*′-((3 hydroxy-5-(hydroxymethyl)-2-methylpyridin-4-yl)methylene)-2-naphthohydrazide	Turn-off fluorescence	1 : 1	NR	530	6.1×10^5	0.87 μM	Cell imaging	1
(2,2′-((1*Z*, 1′*Z*)-(2,2′-(pyrimidine-2,4-diyl)bis(hydrazin-2-yl-1-ylidene))bis(ethan-1-yl-1-ylidene))diphenol)	Turn-on fluorescence	1 : 1	7.0	469	11.82×10^4 (abs) 3.85×10^4 (emiss)	0.83 M	Bacterial cell imaging	28
7-(4′-(Diethylamino)-2′-hydroxybenzylideneimino)-4-methyl coumarin	Turn-on fluorescence	1 : 2	NR	500	1.09×10^6	2.59 μM	NR	55
N,*N*′-Bis(*p*-chlorosallicylidene)-1,2-etheylenediamine	Turn-on fluorescence	2 : 1	6.8	500	6.17×10^9	3.21 μM	NR	56
1-[(2-Pyridin-2-yl-ethylimino)-methyl]- naphthalen-2-ol	Turn-on fluorescence	1 : 2	7.4	452	1.47×10^5	0.45 μM	Cell imaging	57
2-Hydroxynaphthalene-1-carboxaldehyde with tris(2-aminoethyl)amine	Colorimetric & turn-on fluorescence	1 : 1	2.0–10.0	450	1.23×10^7	0.49 μM	NR	58
2-Hydrozinylpyridine with the corresponding aldehyde	Turn-on fluorescence	1 : 1	7.2	545	2.28×10^5	NR	Cell imaging	59
N,*N*′ -Bis(salicylidene)-1,2-phenylenediamine	Turn-on fluorescence	1 : 1	8.0–11.0	450	13.1×10^4	NR	NR	60
2-((2-(Pyrimidin-2-yl)hydrazono)methyl)phenol	Turn-on fluorescence	1 : 2	7	470	6.76×10^6 (emis) 7.58×10^6 (abs)	0.497 μM	Cell imaging	This work

(b)

Nanocomposite/nanoparticle system	Sensor type	pH	Wavelength	Binding constant (M^{-1})	LOD	Application	Ref.
Ag NP	Colorimetric sensor	7	425 nm	NR	3.5 μM	Determination of Zn^{2+} in drinking water	76
Fe_3O_4@SiO_2	Potentiometric detection	7	—	—	1 μM	Detection of Zn^{2+} in tap water	77
MDPA-GNPs	Turn-on Fluorescence	7	425 nm	1.46×10^5 (emission)	0.32 μM	intracellular imaging	78
CMC–CdTe QDs	Turn-on fluorescence	4–8	566 nm	NR	4.5 μM	Cellular imaging	79
Dye assembled upconversion Nanoparticles	Turn-on fluorescence	7.0	475 nm	NR	0.78 μM	*in vitro* and *in vivo* application	80
DPA-P-DTC-CdSe/ZnS QDs	Turn-on fluorescence	7.5	584nm	3.7×10^7 (Zn^{2+}–DPA)	0.7 μM	Stimulated Biological fluid	81
PHP	Turn on	7	470 nm	6.76×10^6 (emis) 7.58×10^6 (abs)	0.497 μM	Cell imaging	This work

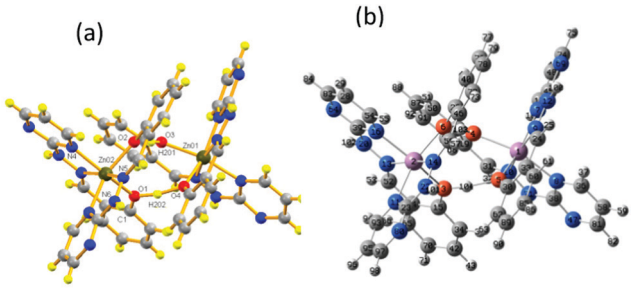

Fig. 8 Comparison between (a) single crystal and (b) optimized structure of the complex.

Time resolved decay analysis

Lifetime measurement was carried out to identify the micro-environment around PHP–Zn^{2+} in solution. In order to realize the photophysics of PHP both in the absence and presence of transition metal ions, time-resolved fluorescence measurements were performed for the complex probe at 470 nm. It is indicated from Fig. 6 that the fluorescence decay behaviour after the initial addition of Zn^{2+} is clearly biexponential, which consists of a short-lived major component (0.23 ns, 96%) arising for the ligand moiety and a minor long-lived component due to the metal–ligand complex (2.33 ns, 4%). Lifetime for both the first and second components decreases gradually with regular addition of Zn^{2+} ions. These data suggest that on gradual addition of Zn^{2+} ions, binding with N and O atoms takes place and the lifetime of the bonded species become shorter, which results in the decrease in lifetime. Thus, the decrease in lifetime is clearly an evidence of excited state metal ligand (PHP) bonding phenomenon.

NMR titration

In addition to the crystal structure, to gain insights into the transformation mechanism of PHP to complex **1**, ^{1}H NMR spectroscopy has been performed using individual addition of Zn^{2+} to the receptor PHP in 1 : 1 equivalent ratio in DMSO-d6. As shown in Fig. 7, upon treatment with Zn^{2+} ion, the ^{1}H NMR spectrum of PHP dramatically changed. A more downfield shift of O–H proton H_a from δ 10.90 to 11.70 ppm confirms the direct binding of oxygen with Zn^{2+}. The existence of H_a peak after saturation also proves that it resides even after zinc binding with the oxygen atom. Simultaneously, amine proton 'H_b' at δ 10.52 ppm shifted to up-field (δ 10.44 ppm) when Zn^{2+} bonded with imine nitrogen, 'N_b' near the mentioned amine group. To further elucidate the zinc connectivity with 'N_b' nitrogen, the H_c proton connected to the adjacent carbon atom of 'N_b' is also shifted after Zn^{2+} addition. A downfield shift of the C–H proton 'H_c' in Schiff base moiety also supported the binding evidence with 'N_b'. 'H_c' proton shifted from δ 8.28 to 8.38 ppm to complete binding with PHP and Zn^{2+}. A downfield shift of aromatic protons H_f and H_g in pyrimidin ring from δ 7.65 to 7.80 ppm and 7.58 to 7.69 ppm, respectively, ascertains that the N_f nitrogen of pyrimidin ring directly involves in the bonding with the metal. Other proton NMR peaks from Fig. 7 remain unaltered as they are not involved in the bonding phenomenon. Hence, the NMR study infers that only oxygen atom, 'N_b' and 'N_f' nitrogen atoms of PHP ligand are involved in binding with zinc to form Complex **1**. Moreover, the shift in ^{1}H NMR peak values became insignificant after the addition of 0.6 equivalent Zn^{2+}, which signifies the 1 : 2 metal–ligand bonding. So, the three bonding sites from each PHP molecule form the complex as observed from the crystal structure.

According to the above experimental results, the binding mechanism of PHP has been successfully discussed, and moreover, a comparison of PHP with some other reported Zn^{2+} Schiff base fluorescent probes is summarized in Table 4(a). Compared with other Schiff base sensors,[1,28,55–60] the interesting factors of PHP ligand were higher binding constant, new synthesis mechanism, and comparable or lower detection limit.

Recently various nanocomposites have been fabricated for sensing diverse materials, *e.g.*, metal ion, anion, uric acid, melamine, 4-hexylresorcinol, 3-methoxyanaline, *etc.* with very precise sensitivity.[61–74] Here, it should be clearly noted that sensitivity of the synthesized sensor PHP is higher and comparable sometimes than previously reported Zn^{2+} sensors based on various nanocomposites or materials (summarized in Table 4(b)). Although sensitivity of nanosensors are very high but in many cases development of such nanosensors are cost effective, low yield, characterization requires high infrastructural facility and sometimes their applications may suffer from toxicity.[75] On the other hand, synthesis of PHP has low cost synthesis route, high yield with high purity, and most importantly, it shows effective cell line penetration as shown in PC-3 cell (Cell imaging section). Therefore,

Table 5 Comparison in geometrical parameters between single crystal structure and optimized DFT structure of Complex **1**

	Crystal optimized structure DFT structure	Crystal structure	Optimized DFT structure
Bond angle (degree)	O1–H202–O4 = 3(O)–104(H)–5(O)	166.96	174.12
	N4–Zn02–N5 = 16(N)–2(Zn)–14(N)	97.09	98.84
	Zn02–O1–H202 = 2(Zn)–3(O)–104(H)	111.98	115.51
	Zn01–O4– H202 = 1(Zn)–5(O)–104(H)	120.17	115.14
	O3– Zn01–O4 = 4(O)–1(Zn)–5(O)	85.30	85.41
Bond length (Å)	O1–H202 = 3(O)–104(H)	1.16	1.09
	O4–H202 = 5(O)–104(H)	1.34	1.43
	Zn02–N5 = 2(Zn)–14(N)	2.13	2.14
	Zn02–O1 = 2(Zn)–3(O)	2.16	2.20
	Zn01–O4 = 1(Zn)–5(O)	2.06	2.05
	O3–H201 = 4(O)–103(H)	0.97	1.04

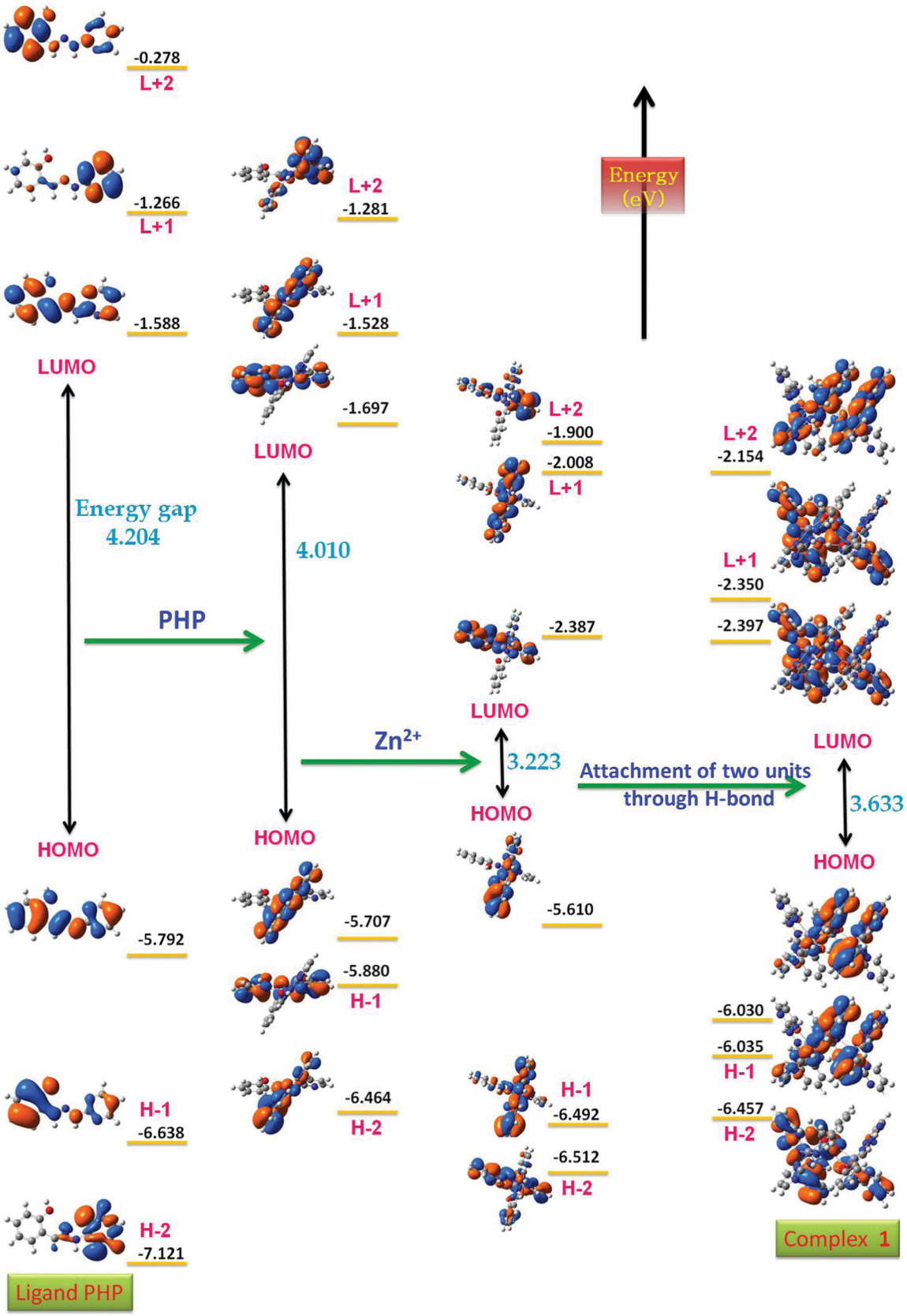

Scheme 2 Frontier Molecular Orbital (FMO) diagram and respective change in energies of ligand PHP to complex **1**.

in a comparative view, PHP can compete with many nanosensors in terms of cost and sensitivity.

Computational calculation

To help elucidate the coordination mode of Zn^{2+} with PHP in solution, the structure of complex **1** has been optimized at the DFT level (Fig. 8). In an aqueous solution, a hydrogen atom attached between two mononuclear units plays a crucial function in the stabilization of the binuclear complex **1**. A comparison of key geometric parameters between the crystal structure and optimized geometry of complex 1 has been inserted in Table 5. The most interesting feature is the O–H bond distance associated with the particular hydrogen atom named as H202 in the crystal structure and 104(H) in the optimized DFT structure, which stitches the two mononuclear units in complex 1. The O–H bond distances in the crystal structure and optimized structures are 1.16 (O1–H202) and 1.09 Å [3(O)–104(H)], respectively, with one mononuclear unit and 1.34 (O4–H202) and 1.43 Å [5(O)–104(H)], respectively, with the other unit. In comparison, H201 or 103(H) hydrogen atom is bonded with only one mononuclear unit having bond distances 0.97 (O3– H201) and 1.04 Å [4(O)–103(H)] for crystal structure and optimized structure, respectively. Moreover, if we look at the O–H–O bond angle (O1–H202–O4 = 166.96° for crystal structure and 3(O)–104(H)–5(O) = 174.12° for optimized structure), then there is a more or less linear arrangement of the bond in both structures. So, the H202 or 104(H) hydrogen atom linked with two oxygen atoms O4–H202 and O1–H202 or 5(O)–104(H) and 3(O)–104(H) for connecting the two units in complex 1, whereas H201 or 103(H) hydrogen atom forms one covalent bond (O3–H201) and 4(O)–103(H) with one mononuclear unit and another hydrogen bond O2···H201 or 6(O)···103(H) with another mononuclear unit. The two PHP ligands are mutually at the right angle (97.09° for crystal structure and 98.84° for optimized structure) to co-ordinate with zinc metal.

Orbital energy level diagrams of these systems using DFT calculations (Scheme 2) near the HOMO/LUMO are useful for monitoring the sensor's response and Zn^{2+} ion selectivity towards the ligand. If we observe the subsequent energy changes in frontier molecular orbital from PHP sensor to 2 : 1 PHP–Zn^{2+} mononuclear complex, there is a regular decrease in the HOMO–LUMO energy gap. In addition, the formation of mononuclear to binuclear chelated complex **1** through H-atom results in a stabilization of both HOMO and LUMO energy levels. The maximum stabilization of HOMO and LUMO in complex **1** infers the H-bonded binuclear complex is the most stable structure. For complex **1**, one can see the frontier molecular orbital spread above the entire π-conjugated structure. To facilitate the UV-vis absorption study and photophysical properties of complex **1**, time dependent DFT (TD-DFT) calculations were also performed in association with DFT. The calculated absorption at 383 nm well concurs with the experimental results of UV-vis at 383 nm. This transition occurred due to the ligand to metal charge transfer process. The distribution of electron cloud over the whole PHP structure was also affected after the formation of binuclear complex **1**. Therefore, theoretical calculations in point of electronic and spectral arrangement with experimental correlation specified that PHP ligand performs as a suitable sensor of Zn^{2+} to form rarely H-stitched binuclear complex **1**.

Cell imaging

For evaluation of the biological application of our sensor PHP, further study was extended to access its possible utility for *in vitro* fluorescence imaging in human prostate carcinoma (PC-3) cells using a confocal microscope. First of all, the cultured PC-3 cells were seeded on a 22 mm cover slip in six well plates. After that to evaluate *in vivo* zinc bio-imaging utilities, in one plate PHP (15 μM) only was incubated (37 °C for 12 h) with live PC-3 cells, and in another plate, PC-3 cells were incubated (37 °C for 12 h) with 30 μM exogenous Zn^{2+} by means of a zinc carrier, sodium pyrithione. It can be seen from Fig. 9 that PC-3 cells when incubated with only PHP, show very feeble background fluorescence. However, zinc treated cells display a strong fluorescence spread all over the cells but

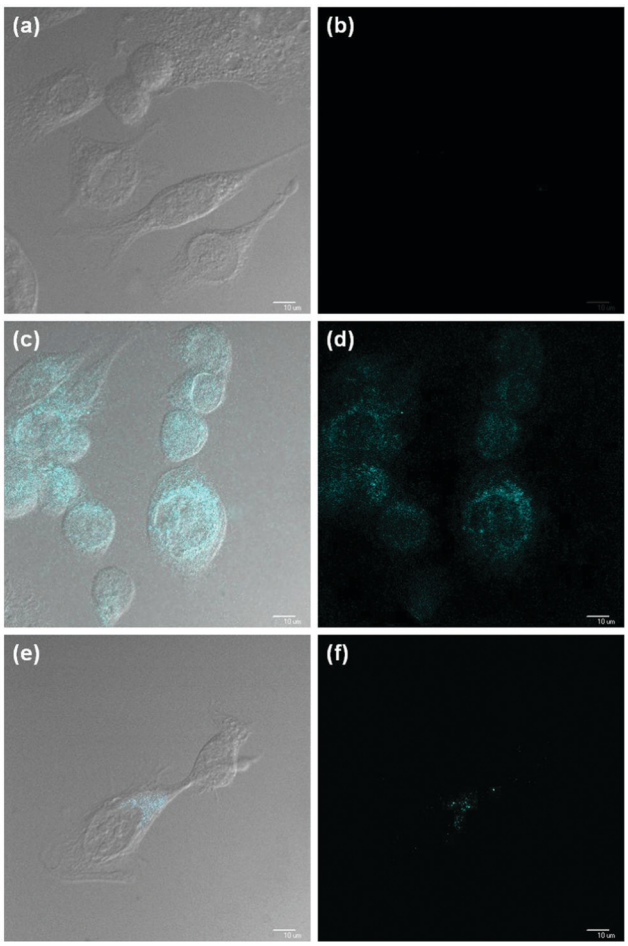

Fig. 9 Fluorescent imaging of PC-3 cells using confocal microscope. Cells incubated with only 20 μM PHP (a) gray field (b) dark field. In images (c) and (d), the cells supplemented with 20 μM of the PHP and then loaded with 30 μM of Zn^{2+} and sodium pyrithione as a zinc carrier. The cell image in (e) and (f) incubated for 20 min before imaging with TPEN (100 μM).

mostly concentrated around the cell nucleus. However, in contrast, the subsequent addition of TPEN, a zinc chelator decreases the intracellular fluorescence intensity signifying the fluorescence signals are nothing but the consequences of fluorescent complex **1** formed after the external addition of zinc ion with PHP. So, it is very crucial to conclude that PHP ligand has reversibility and high cell permeability efficiency, which can be used as a bio-sensor to investigate the intracellular Zn^{2+} concentrations and bioactivity in living cells.

Hence, the above discussion from all sections signifies that the newly designed low cost PHP ligand can selectively respond to Zn^{2+} in the presence of other metal ion mixtures with the fluorescence ''turn-on'' action. The new crystal formed by the ligand PHP with Zn^{2+} is rare and unique, as a single H-atom stitched two mononuclear units only through the ligands to form a giant binuclear complex **1** without any metal–metal linkage. Most importantly, this cheap PHP sensor has the cell penetration ability with significant reversibility to justify its application in biophysical studies.

Conclusion

In summary, we have successfully fabricated a highly pure new PHP chemical sensor in a simple, convenient, and economical approach to detect Zn^{2+} in the presence of other metal ions in solution. Analytical performances of PHP sensor with Zn^{2+} were examined using absorption, fluorescence, NMR titration, and computational techniques in terms of sensitivity, detection limit, stability, and separation. In solution, the PHP ligand formed an uncommon H-stitched unique binuclear solid crystal complex **1** with Zn^{2+}, which is reported for the first time. The supramolecular hydrogen bonding and C–H$\cdots\pi$ interactions are well explained and demonstrated in various supramolecular structures formed by this rare crystal. In addition, the sensor was applied in the successful detection of Zn^{2+} in real biological human prostate carcinoma cell samples. This report has provided extensive research activities, including convenient synthesis, experimental and theoretical sensing mechanism with detailed binding site investigation, and *in vitro* application. The main advantages of our study over the other reported works are easy high purity simple synthesis, cost effective, ambient conditions and operation without using highly sophisticated instruments. So, this novel approach introduces a new route for efficient and selective chemical sensor development to address healthcare and environmental issues.

Conflicts of interest

There are no conflicts to declare.

Acknowledgements

The authors are very much thankful to Prof. Subhash Ch. Bhattacharya and his Photo Laboratory in Jadavpur University for providing different laboratory facilities. Author Soumya Sundar Mati greatly acknowledges SERB, India, for grant in project TAR/2019/000030. S. K. is thankful to The Bhawanipur Education Society College for providing a research grant (Project No. BESC/RPC/2019–2020/SC1/02).

References

1 T. Anand, A. K. Sk and S. K. Sahoo, *Photochem. Photobiol. Sci.*, 2018, **17**, 414–422.
2 A. Mayor-Ibarguren, C. Busca-Arenzana and Á. Robles-Marhuenda, *Front. Immunol.*, 2020, **11**, 1736.
3 Y. Upadhyay, T. Anand, L. Thilak Babu, P. Paira, G. Crisponi, A. K. Sk, R. Kumar and S. K. Sahoo, *Dalton Trans.*, 2018, **47**, 742–749.
4 M. Kiani, M. Bagherzadeh, S. Meghdadi, N. Rabiee, A. Abbasi, K. Schenk-Joß, M. Tahriri, L. Tayebi and T. J. Webster, *New J. Chem.*, 2020, **44**, 11841–11852.
5 K. Tayade, B. Bondhopadhyay, H. Sharma, A. Basu, V. Gite, S. Attarde, N. Singh and A. Kuwar, *Photochem. Photobiol. Sci.*, 2014, **13**, 1052–1057.
6 M. Maares and H. Haase, *Nutrients*, 2020, **12**, 762.
7 A. Maji, S. Pal, S. Lohar, S. K. Mukhopadhyay and P. Chattopadhyay, *New J. Chem.*, 2017, **41**, 7583–7590.
8 S. Chowdhury, B. Rooj, A. Dutta and U. Mandal, *J. Fluoresc.*, 2018, **28**, 999–1021.
9 V. Kumar, A. Kumar, U. Diwan and K. K. Upadhyay, *Dalton Trans.*, 2013, **42**, 13078–13083.
10 D. Yun, J. Byeong Chae, H. So, H. Lee, K. Kim and C. Kim, *New J. Chem.*, 2020, **44**, 442–449.
11 Y. Yang, C. Ma, Y. Zhang, Q. Xue, J. Ru, X. Liu and H. Guo, *Anal. Methods*, 2018, **10**, 1833–1841.
12 X. Peng, X. Tang, W. Qin, W. Dou, Y. Guo, J. Zheng, W. Liu and D. Wang, *Dalton Trans.*, 2011, **40**, 5271–5277.
13 X. Gao, X. Zhuang, C. Tian, H. Liu, W. Lai, Z. Wang, X. Yang, L. Chen and A. L. Rogach, *Sens. Actuators, B*, 2020, **307**, 127626.
14 Y. Li, X. Hu, X. Zhang and Y. Huang, *Anal. Chim. Acta*, 2018, **1024**, 145–152.
15 A. Gomathi, P. Viswanathamurthi and K. Natarajan, *J. Photochem. Photobiol., A*, 2019, **370**, 75–83.
16 S. J. Malthus, S. A. Cameron and S. Brooker, *Inorg. Chem.*, 2018, **57**(5), 2480–2488.
17 U. A. Fegade, S. K. Sahoo, A. Singh, N. Singh, S. B. Attarde and A. S. Kuwar, *Anal. Chim. Acta*, 2015, **872**, 63–69.
18 T. Anand, A. K. Sk and S. K. Sahoo, *ChemistrySelect*, 2017, **2**, 7570–7579.
19 S. Chall, S. S. Mati, S. Konar, D. Singharoy and S. Chandra Bhattacharya, *Org. Biomol. Chem.*, 2014, **12**, 6447–6456.
20 M. S. R. Prabhu, *Int. J. Res. Anal. Rev.*, 2018, **5**(2), 797–805.
21 H. Naeimi, H. Sharghi, F. Salimi and K. Rabiei, *Heteroat. Chem.*, 2008, **19**, 43–47.
22 M. M. Rahman, M. M. Hussain, M. N. Arshad, M. R. Awual and A. M. Asiri, *New J. Chem.*, 2019, **43**, 9066–9075.
23 V. K. Gupta, A. K. Singh and L. K. Kumawat, *Sens. Actuators, B*, 2014, **204**, 507–514.

24 Y. He, J. Yin and G. Wang, *Chem. Heterocycl. Compd.*, 2018, **54**, 146–152.
25 E. Horak, R. Vianello, M. Hranjec and I. M. Steinberg, *Supramol. Chem.*, 2018, **0278**, 1–10.
26 A. M. Abu-Dief and I. M. Mohamed, *Beni-Suef Univ. J. Basic Appl. Sci.*, 2015, **4**, 119–133.
27 A. L. Berhanu, Gaurav, I. Mohiuddin, A. K. Malik, J. S. Aulakh, V. Kumar and K. H. Kim, *Trends Anal. Chem.*, 2019, **116**, 74–91.
28 S. S. Mati, S. Chall, S. Konar, S. Rakshit and S. C. Bhattacharya, *Sens. Actuators, B*, 2014, **201**, 204–212.
29 T. A. Sheikh, M. N. Arshad, M. M. Rahman, A. M. Asiri, H. M. Marwani, M. R. Awual and W. A. Bawazir, *Inorg. Chim. Acta*, 2017, **464**, 157–166.
30 R. M. Kamel, A. Shahat, W. H. Hegazy, E. M. Khodier and M. R. Awual, *J. Mol. Liq.*, 2019, **285**, 20–26.
31 M. R. Awual, M. M. Hasan, J. Iqbal, A. Islam, M. A. Islam, A. M. Asiri and M. M. Rahman, *Microchem. J.*, 2020, **154**, 104585.
32 L. Pauling, *J. Am. Chem. Soc.*, 1931, **53**, 3225–3237.
33 J. Djukic, J. Sortais, L. Barloy, N. Pannetier, C. Sirlin and M. Pfeffer, *Organometallics*, 2012, **31**, 2821–2828.
34 V. A. Yartys, R. V. Denys, J. P. Maehlen, C. Frommen, M. Fichtner, B. M. Bulychev and H. Emerich, *Inorg. Chem.*, 2007, **46**, 1051–1055.
35 C. Femoni, M. C. Iapalucci, G. Longoni and S. Zacchini, *Dalton Trans.*, 2011, **40**, 8685–8694.
36 N. Wang, M. Wang, L. Chena and L. Sun, *Dalton Trans.*, 2013, **42**, 12059–12071.
37 M. Pérez-Jiménez, N. Curado, C. Maya, J. Campos, E. Ruiz, S. Álvarez and E. Carmona, *Chem. – Eur. J.*, 2021, **27**(21), 6569–6578.
38 J. Chesterfield, J. F. W. McOmie and E. R. Sayer, *J. Chem. Soc.*, 1955, 3478–3481.
39 G. M. Sheldric, *SHELXS-97 and SHELXL-97*, University of Göttingen, Germany, 1997.
40 W. Khon and L. J. Sham, *Phys. Rev.*, 1965, **140**, A1133–A1138.
41 A. D. Becke, *J. Chem. Phys.*, 1993, **98**, 5648–5652.
42 S. S. Mati, S. Chall, S. Rakshit and S. C. Bhattacharya, *J. Fluoresc.*, 2015, **25**, 341–353.
43 S. S. Mati, S. Sarkar, P. Sarkar and S. C. Bhattacharya, *J. Phys. Chem. A*, 2012, **116**, 10371–10382.
44 J. Frisch, G. W. Trucks, G. W. Trucks, H. B. Schlegel, G. E. Scuseria, M. A. Robb, J. R. Cheeseman, G. Scalmani, V. Barone, B. Mennucci, G. A. Petersson, H. Nakatsuji, M. Caricato, X. Li, H. P. Hratchian, A. F. Izmaylov, J. Bloino, G. Zheng, J. L. Sonnenberg, M. Hada, M. Ehara, K. Toyota, R. Fukuda, J. Hasegawa, M. Ishida, T. Nakajima, Y. Honda, O. Kitao, H. Nakai, T. Vreven, J. A. Montgomery, Jr., J. E. Peralta, F. Ogliaro, M. Bearpark, J. J. Heyd, E. Brothers, K. N. Kudin, V. N. Staroverov, T. Keith, R. Kobayashi, J. Normand, K. Raghavachari, A. Rendell, J. C. Burant, S. S. Iyengar, J. Tomasi, M. Cossi, N. Rega, J. M. Millam, M. Klene, J. E. Knox, J. B. Cross, V. Bakken, C. Adamo, J. Jaramillo, R. Gomperts, R. E. Stratmann, O. Yazyev, A. J. Austin, R. Cammi, C. Pomelli, J. W. Ochterski, R. L. Martin, K. Morokuma, V. G. Zakrzewski, G. A. Voth, P. Salvador, J. J. Dannenberg, S. Dapprich, A. D. Daniels, O. Farkas, J. B. Foresman, J. V. Ortiz, J. Cioslowski and D. J. Fox, *Gaussian 09, Revision B. 01M*, Gaussian, Inc., Wallingford CT, 2010.
45 D. Cremer and J. A. Pople, *J. Am. Chem. Soc.*, 1975, **97**, 1354–1358.
46 V. K. Gupta, A. K. Singh, M. R. Ganjali, P. Norouzi, F. Faridbod and N. Mergu, *Sens. Actuators, B*, 2013, **182**, 642–651.
47 S. Liu, C. Bi, Y. Fan, Y. Zhao, P. Zhang, Q. Luo and D. Zhang, *Inorg. Chem. Commun.*, 2011, **14**, 1297–1301.
48 T. Mistri, M. Dolai, D. Chakraborty, A. R. Khuda-Bukhsh, K. K. Das and M. Ali, *Org. Biomol. Chem.*, 2012, **10**, 2380–2384.
49 Z. Xu, J. Yoon and D. R. Spring, *Chem. Soc. Rev.*, 2010, **39**, 1996–2006.
50 F. Zhu, H. Yuan, W. H. Chan and A. W. M. Lee, *Org. Biomol. Chem.*, 2010, **8**, 3957–3964.
51 M. Tajbakhsh, G. B. Chalmardi, A. Bekhradnia, R. Hosseinzadeh, N. Hasani and M. A. Amiri, *Spectrochim. Acta, Part A*, 2018, **189**, 22–31.
52 J. W. Nugent, H. Lee, H. Lee, J. H. Reibenspies and R. D. Hancock, *Chem. Commun.*, 2013, **49**, 9749–9751.
53 Q. You, P. Chan, W. Chan, S. C. K. Hau, A. W. M. Lee, N. K. Mak, T. C. W. Mak and R. N. S. Wong, *RSC Adv.*, 2012, **2**, 11078–11083.
54 J. Qin, L. Fan and Z. Yang, *Sens. Actuators, B*, 2016, **228**, 156–161.
55 J. C. Qin, L. Fan and Z. Y. Yang, *Sens. Actuators, B*, 2016, **228**, 156–161.
56 K. Kaur, S. Chaudhary, S. Singh and S. K. Mehta, *J. Lumin.*, 2015, **160**, 282–288.
57 B. Naskar, R. Modak, D. K. Maiti, S. K. Mandal, J. K. Biswas, T. K. Mondal and S. Goswami, *Polyhedron*, 2016, **117**, 834–846.
58 W. H. Hsieh, C. F. Wan, D. J. Liao and A. T. Wu, *Tetrahedron Lett.*, 2012, **53**, 5848–5851.
59 J. Wang, Y. Li, E. Duah, S. Paruchuri, D. Zhou and Y. Pang, *J. Mater. Chem. B*, 2014, **2**, 2008–2012.
60 T. S. Singh, P. C. Paul and H. A. R. Pramanik, *Spectrochim. Acta, Part A*, 2014, **121**, 520–526.
61 M. R. Awual and M. M. Hasan, *J. Mol. Liq.*, 2019, **294**, 111679.
62 M. M. Alam, A. M. Asiri, M. T. Uddin, Inamuddin, M. A. Islam, M. R. Awual and M. M. Rahman, *New J. Chem.*, 2019, **43**, 4849–4858.
63 R. Awual, T. Yaita, T. Kobayashi, H. Shiwaku and S. Suzuki, *J. Environ. Chem. Eng.*, 2020, **4**(2), 103684.
64 S. Khandakera, Y. Toyoharab, G. C. Sahac, M. R. Awuald and T. Kubaf, *J. Water Process. Eng.*, 2020, **33**, 101055.
65 A. Islama, T. Ahmed, M. R. Awual, A. Rahman, M. Sultana, A. A. Aziz, M. U. Monira, S. H. Teoe and M. Hasan, *J. Cleaner Prod.*, 2020, **244**, 118815.
66 A. Islam, S. H. Teo, M. R. Awual and Y. H. Taufiq-Yap, *J. Cleaner Prod.*, 2019, **238**, 117887.
67 M. M. Alam, A. M. Asiri, M. T. Uddin, M. A. Islam, M. R. Awual and M. M. Rahman, *New J. Chem.*, 2019, **43**, 8651–8659.

68 T. A. Sheikh, M. M. Rahman, A. M. Asiria, H. M. Marwani and M. R. Awual, *J. Ind. Eng. Chem.*, 2018, **66**, 446–455.
69 M. R. Awual, M. M. Hasan, A. M. Asiri and M. M. Rahman, *J. Mol. Liq.*, 2019, **283**, 704–712.
70 M. R. Awual, M. M. Hasan, A. Islam, A. M. Asiri and M. M. Rahman, *J. Mol. Liq.*, 2020, **298**, 112035.
71 A. Shahat, H. M. A. Hassan, M. F. El-Shahat, O. E. Shahawy and M. R. Awual, *Chem. Eng. J.*, 2018, **334**, 957–967.
72 M. R. Awual, M. M. Hasan, A. Islam, M. M. Rahman, A. M. Asiri, M. A. Khaleque and M. C. Sheikh, *J. Cleaner Prod.*, 2019, **228**, 778–785.
73 M. R. Awual, M. M. Hasan, J. Iqbal, A. Islam, M. A. Islam, S. Khandaker, A. M. Asiri and M. M. Rahman, *J. Environ. Chem. Eng.*, 2020, **8**, 103591.
74 M. M. Rahman, T. A. Sheikh, A. M. Asiri and M. R. Awual, *New J. Chem.*, 2019, **43**, 4620–4632.
75 R. Kaur, S. K. Sharma and S. K. Tripathy, Advantages and Limitations of Environmental Nanosensors, *Advances in Nanosensors for Biological and Environmental Analysis*, Elsevier, 2019, ch. 7, pp. 119–132.
76 M. Ihsan, A. Niaz, A. Rahim, M. Iqbal Zaman, M. B. Arain, Sirajuddin, T. Sharifa and M. Najeeba, *RSC Adv.*, 2015, **5**, 91158–91165.
77 A. A. Bazrafshan, S. Hajati and M. Ghaedi, *RSC Adv.*, 2015, **5**, 105925–105933.
78 D. Li, Y. Ma, H. Duan, F. Jiang, W. Deng and X. Ren, *Anal. Chim. Acta*, 2018, **1038**, 148–156.
79 Q. Ma, Z.-H. Lin, N. Yang, Y. Li and X.-G. Su, *Acta Biomater.*, 2014, **10**, 868–874.
80 J. Peng, W. Xu, C. L. Teoh, S. Han, B. Kim, A. Samanta, J. C. Er, L. Wang, L. Yuan, X. Liu and Y.-T. Chang, *J. Am. Chem. Soc.*, 2015, **137**, 2336–2342.
81 H. Xu, Z. Wang, Y. Li, S. Ma, P. Hu and X. Zhong, *Analyst*, 2013, **138**, 2181–2191.